Bulletin of the Seismological Society of America, Vol. 88, No. 1, pp. 170–182, February 1998

Determination of $\Delta\sigma$ and κ_0 from Response Spectra of Large Earthquakes in Greece

by Basil N. Margaris and David M. Boore

Abstract We fit an ω^{-2} model to response spectra from eight recent Greek earthquakes ranging in size from $\mathbf{M} = 5.8$ to $\mathbf{M} = 6.9$. The diminution parameter κ_0 was determined for each site, with a value near 0.06 for a typical soil site. The stress parameter ($\Delta\sigma$) showed little variation from earthquake to earthquake and had a mean value of 56 bars over all earthquakes. Predictions of peak velocity, peak acceleration, rupture duration, and fault length using the derived stress parameters are consistent with observations. Frequency-dependent site amplifications were included in all estimates; the combined effect of amplification and attenuation had a maximum value close to a factor of 2.5 for a typical soil site, relative to the motions at the surface of a perfectly elastic uniform half-space composed of materials near the source. The results form the foundation for predictions of strong motions in Greece for distances and magnitudes other than those for which data are available.

Introduction

A strong-motion network has been installed and maintained for the last two decades in Greece (Anagnostopoulos *et al.,* 1985; Theodulidis *et al.,* 1986; Margaris *et al.,* 1990; Stavrakakis *et al.,* 1992), and a number of strong earthquakes and their aftershocks have been recorded by the accelerographs in the network. Based on these strong-motion data, empirical relationships of peak and spectral amplitudes as a function of magnitude, distance, and geological conditions have been derived in Greece (Theodulidis and Papazachos, 1992). As in other regions, however, the empirical data do not adequately define ground motions close to large earthquakes. In addition, data are wholly lacking for a number of regions of Greece.

To overcome the lack of critical data, reliance must be placed on theoretical models for the interpolation and extrapolation of the existing data. One such model is the stochastic model of Hanks and McGuire (1981), which is commonly used to extend ground-motion predictions beyond those based solely on empirical data analysis (e.g., Boore, 1983, 1996; Boore and Atkinson, 1987; Atkinson and Boore, 1997; Toro *et al.,* 1997). The high-frequency ground motions predicted by this model are sensitive to several parameters, the most important of which are $\Delta\sigma$ (the stress parameter) and κ_0 (the high-frequency diminution parameter). The purpose of this article is to determine these parameters for earthquakes in Greece by fitting observed response spectra with a single corner-frequency source model, after accounting for site amplification. A similar study was conducted by Papastamatiou *et al.,* (1993), using data from generally smaller earthquakes than in our study (two earthquakes are common to both studies).

We measured κ for each recording. Lacking detailed site-specific soil amplification, we assigned each site to one of three site classes and applied amplification filters derived from the analysis of strong-motion recordings in California. In our formulation, κ_0 is given by the measured κ after correction for site amplification and whole-path attenuation. The combined effect of amplification and high-frequency near-site attenuation ranges from a factor of 1.5 for the rock sites to a factor approaching 3.0 for the softer soil sites.

The $\Delta\sigma$ found from matching pseudorelative-velocity response spectra (PSV) are consistent with Fourier-amplitude spectra, peak acceleration, and peak velocity. In addition, the source size and duration estimated from this stress parameter for each earthquake are consistent with those estimated by other means.

Data

We used strong-motion data from a number of earthquakes in Greece. Because the source characteristics of aftershocks may differ from those of mainshocks (e.g., Boore and Atkinson, 1989), we considered only data from mainshocks. In addition, to avoid complications due to path effects, we restricted the data to the closest recordings (all of which were less than 35 km from the fault). With these restrictions, we used data from seven mainshocks, each with only one or two recordings (unlike the empirical regression-analysis study of Theodulidis and Papazachos, 1992, which used data from 36 earthquakes). A map of the event locations is given in Figure 1, and earthquake and station information

are contained in Tables 1 and 2, respectively. We considered only the horizontal components; no rotations were made of the components.

The 1978 Thessaloniki earthquake (shown in the top two panels of Fig. 2) was a double event (Papazachos *et al.*, 1980; Soufleris and Stewart, 1981), and we treated the two events (A and B) as separate events. We apportioned the overall moment of the event into two parts, according to the ratio of the long-period spectra for the windowed portions of events A and B shown in Figure 2.

Because we matched spectral amplitudes and shapes, it is important to account for site geology. Theodulidis and Papazachos (1992) classified accelerograph sites in Greece into two broad categories: "rock" and "alluvium," following the methodology proposed by Trifunac and Brady (1975). Recent studies have shown that the two site categories do not fully characterize the soil conditions in Greece (Pitilakis *et al.*, 1996). For our study, we have assigned each site to one of three site classes—A, B, or C—of Boore *et al.*, (1993). These site classes are defined in terms of shear-wave velocity averaged over the top 30 m (V_{30} greater than 750 m/sec for A, between 360 and 750 m/sec for B, and between 180 and 360 m/sec for C). We based our assignments on the few available downhole shear-velocity logs and the similarity of surficial geology to sites in California for which measurements of shear-wave velocity are available.

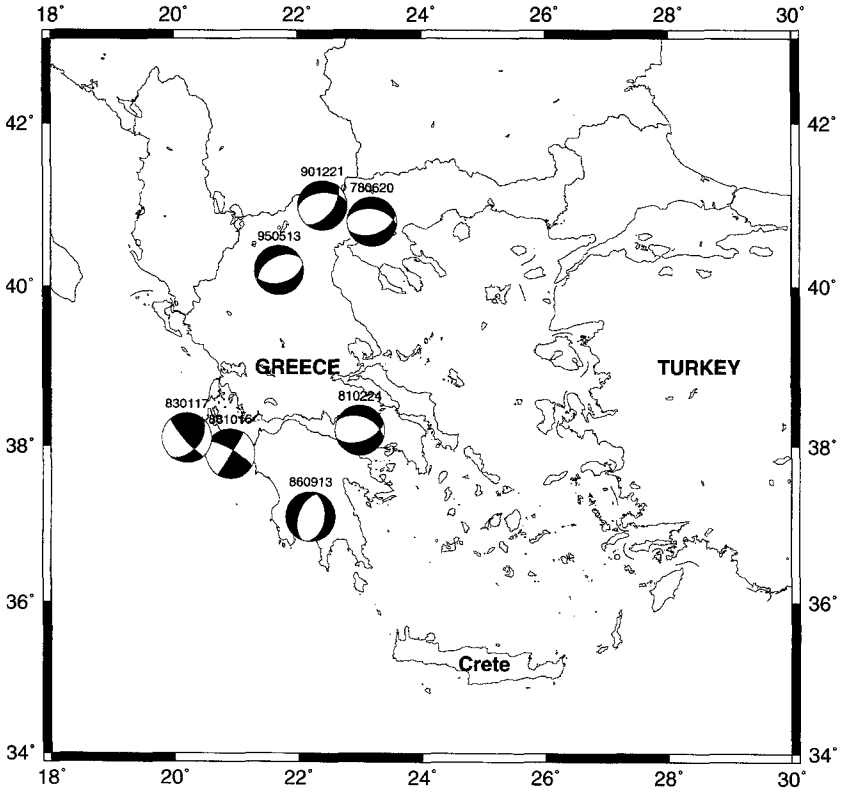

Figure 1. Map of Greece, showing earthquake locations and focal mechanism, as well as year, month, and day of each event.

Table 1
Earthquake Information

Earthquake Code	Date (yymmdd)	Time (hhmmss)	Geographical Name	Fault Type	Fault Leng. (km)	Depth (km)	*Mo** (dyn-cm)	M	Stations
THEA	780620	200321	Thessaloniki	normal(1)	—	—	(0.63*10**25)	(5.8)	THE
THEB	780620	200321	Thessaloniki	normal(1)	30(1)	10	4.4 *10**25(2)	6.4	THE
KOR_	810224	205338	Korinthos	normal (3)	29(4)	6	9.0 *10**25(2)	6.6	KOR
ARG_	830117	124129	Argostoli	strike slip(5)	65(5)	6	23.5*10**25(2)	6.9	ARG
KAL_	860913	172434	Kalamata	normal(6)	15(6)	6	0.98*10**25(2)	6.0	KAL
KYL_	881016	123406	Kyllini	strike slip(2)	17(7)	13	0.75*10**25(2)	5.9	AML, ZAK
GRI_	901221	065744	Griva	normal(8)	15(8)	18	1.7 *10**25(2)	6.1	EDE, KIL
KOZ_	950513	084721	Kozani	normal(9)	30(9)	9	7.6 *10**25(2)	6.6	KOZ

*The moments are based on various non-strong-motion, long-period recordings. (1) Papazachos *et al.* (1980). (2) Papazachos *et al.* (1997). (3) Papazachos *et al.* (1984). (4) Papazachos and Papazachou (1989). (5) Scordilis *et al.* (1985). (6) Papazachos *et al.* (1988). (7) Karakostas *et al.* (1993). (8) Panagiotopoulos *et al.* (1993). (9) Papazachos *et al.* (1995).

Table 2
Station and Recording Information

Station Code	Station Name	Geogr. Coord. N	Geogr. Coord. E	Site Class	Instrument Type	Instrument Owner	Filters (Hz)* Low-cut	Filters (Hz)* High-cut	Organiz. Proc.SMD
AML	Amaliada	37.800	21.333	C	SMA-1	NOA(7)	0.07–0.30	25.–27.	ITSAK(7)
ARG	Argostoli	38.167	20.483	B	SMA-1	ITSAK(4)	0.90–1.03	25.–25.	ITSAK(5)
EDE	Edessa	40.800	22.050	C	SMA-1	ITSAK(8)	0.07–0.35	25.–27.	ITSAK(8)
KAL	Kalamata	37.033	22.120	C	SMA-1	ITSAK(6)	0.10–0.30	30.–32.	ITSAK(6)
KIL	Kilkis	40.983	22.883	B	SMA-1	ITSAK(8)	0.08–0.35	25.–27.	ITSAK(8)
KOR	Korinth	37.933	22.927	C	SAM-1	NOA(1)	0.05–0.125	25.–25.	TUA(3)
KOZ	Kozani	40.300	21.783	A	SMA-1	ITSAK(9)	0.13–0.36	25.–27.	ITSAK(9)
THE	Thessaloniki	40.633	22.933	C	SMA-1	NOA(1)	—	—	TUA(2)
ZAK	Zakynthos	37.783	20.883	C	SMA-1	ITSAK(7)	0.12–0.23	25.–27.	ITSAK(7)

*End points of a ramp from values of 0.0 to 1.0.

(1) Stavrakakis *et al.* (1992). (2) Carydis *et al.* (1983). (3) Carydis *et al.* (1982). (4) Anagnostopoulos *et al.* (1985). (5) Margaris *et al.* (1990). (6) Anagnostopoulos *et al.* (1987). (7) Margaris *et al.* (1993). (8) Pitilakis *et al.* (1992). (9) Theodulidis and Lekidis (1996).

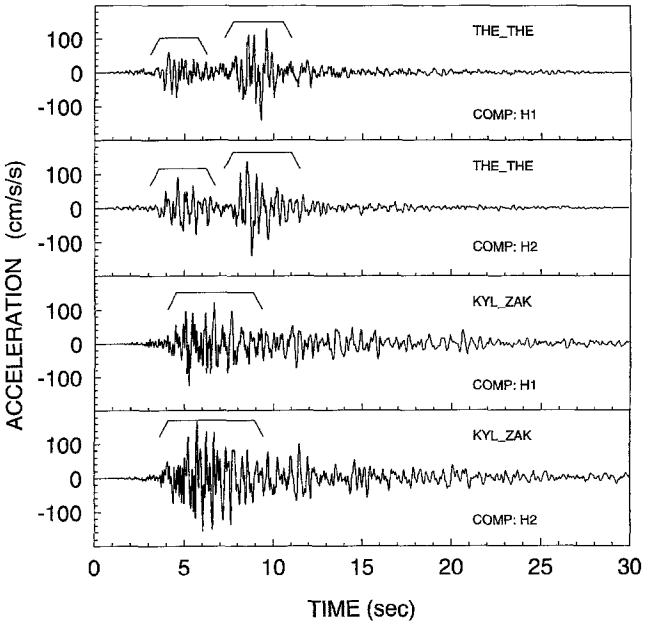

Figure 2. Examples of horizontal-component records and the window used for computing the Fourier-amplitude spectrum needed in the determination of κ. The component designations "H1" and "H2" correspond to motions in the direction of the long and narrow edges of the instrument case. No rotation of components was done in the analysis. The Thessaloniki earthquake (top two traces) was a double event, and the figures shows how we divided the accelerogram into each event. For all but the Thessaloniki recordings, the PSV were computed from the whole record; for the Thessaloniki records, the PSV was determined using the sections indicated in the figure.

The site classes are given in Table 2. We discuss the site amplifications chosen for each site class in a later section.

Fourier amplitude spectra (FAS) and 5%-damped PSV, as well as peak acceleration and peak velocity, were computed from the horizontal-component accelerograms; these are the basic data used in deriving the stochastic-model parameters. The Fourier spectra, which can be sensitive to record length, were computed for windows that included the bulk of the *S*-wave arrival (e.g., Fig. 2) and were not smoothed. The PSV were computed for the whole record.

Method of Analysis

Basic Procedure

Our primary goal was to determine the parameter $\Delta\sigma$ in the following description of the radiated spectrum [see Joyner and Boore (1988) and Boore (1996) for more details]:

$$R(f) = CS(f)A(f)D(f)I(f), \quad (1)$$

where C is a scaling factor, $S(f)$ is the source spectrum, $A(f)$ is the site amplification factor, $D(f)$ is the diminution function, and $I(f)$ is a factor that includes such things as instrument-response factor and filters used in processing. $\Delta\sigma$ is a key parameter that controls the spectral shape and the amplitude of the source spectrum $S(f)$, for which we adopted the following standard expression:

$$S(f) = M_0/[1 + (f/f_0)^2], \quad (2)$$

where M_0 is the seismic moment and f_0 is the corner frequency, given by

$$f_0 = 4.9 \times 10^6 \beta(\Delta\sigma/M_0)^{1/3}, \quad (3)$$

where β, $\Delta\sigma$, and M_0 have units of km/sec, bars, and dyne-cm, respectively. Several studies have proposed more complicated source spectra than given in equation (2) (e.g., Joyner, 1984; Atkinson and Silva, 1997). Our study was directed at obtaining parameters that can be used to predict ground motions in the frequency range of most interest to earthquake engineers, and we found that the simpler form gives adequate predictions of the observed strong motion. As shown later, we did find a bias between observed and

simulated results, which could be due to inadequacies in a number of things, including the source model and the site amplification. We have too few data to derive improved source or site terms, and therefore, we recommend that the bias factor be used as a correction factor for the model used in the simulations.

Another parameter that we determined in this study, on a site-by-site basis, is κ_0, which controls the path-independent high-frequency decay of the spectrum. The diminution function is given by

$$D(f) = e^{-\pi(r/Q(f)\beta + \kappa_0)f}. \quad (4)$$

The path-dependent part of the diminution is controlled by the function $Q(f)$. The fault-to-station distances (r) in our study are relatively small, and therefore, $Q(f)$ does not influence the results significantly.

The amplification factor $A(f)$ strongly controls the derived values of $\Delta\sigma$; we devote the next section to the choices of $A(f)$ for the various sites.

The values for the parameters of equation (1) used in this study are summarized in Table 3. See Boore (1996) for an explanation of those parameters in Table 3 not discussed above.

Our analysis started with determining parameters for the low-cut filters used in the processing; this was followed by estimating κ_0 for each recording. We then used the stochastic model (Boore, 1983, 1996) to simulate PSV for this value of κ_0 and a suite of $\Delta\sigma$. The observed and simulated PSV were compared visually to provide a subjective assessment of the adequacy of the single corner-frequency, ω^{-2}, source model. A quantitative estimate of the "best" stress parameter was determined by finding the value of $\Delta\sigma$ that minimized a measure of misfit between the observed and simulated PSV.

We checked the Fourier-amplitude spectrum and the peak ground acceleration and peak ground velocity for consistency with the derived stress parameters, but we used the PSV as the main datum from which $\Delta\sigma$ is determined. The reasons for this are several: (1) PSV is more closely related to engineering needs than is FAS; (2) PSV is not sensitive to window length, as is FAS; and (3) we desire a model that provides a reasonable approximation over a wide frequency range, and this is best determined by fitting a spectrum rather than a few peak ground-motion parameters.

Table 3
Parameters of the Stochastic Model

Source Properties
• Material properties: $\rho = 2.7$ gm/cm^3, $\beta = 3.4$ km/sec [ρ and β have been taken from Papazachos (1990).]
• Single-corner frequency ω^{-2} spectra, with stress parameters ($\Delta\sigma$) as given in Figure 5 and Table 5.
Path Properties
• Q: $Q = 275(f/0.1)^{-2.0}$ $f \leqq 0.2$; $Q = 88\,(f/1.0)^{+0.9}$ $f \geqq 0.6$ [Q for $0.2 < f < 0.6$ determined from power-law fit to values of Q at $f = 0.2$ and $f = 0.6$ Hz (see Fig. 3 in Boore, 1996). The Q function is that given in Boore (1984); it is in good agreement with local relations of Q in Greece (Hatzidimitriou, 1993, 1995).]
• $1/r$ geometrical spreading
• Duration = $1/f_0 + 0.05r$
Site Properties
• Partition factor = 0.71
• Radiation coefficient = 0.63
• Free surface factor = 2.0
• Site amplification and kappa on a site-by site basis, as given in Tables 2, 4, and 5.

Choice of Site Amplification Filter, $A(f)$

Unfortunately, no detailed and systematic studies have been conducted in estimating frequency-dependent amplification factors for the alluvium soil conditions at accelerograph sites in Greece. Some studies, mainly following some strong earthquakes or as a result of detailed geophysical–geotechnical projects, have been carried out at some of the class C sites that provided data for this study (Pitilakis *et al.*, 1996). At station THE (Table 2), a mean amplification factor from 1.5 to 3.5 was estimated by Raptakis *et al.* (1994) and Lachet *et al.* (1995) for a frequency band 1 to 10 Hz. Studies after the destructive 13 September 1986, Kalamata earthquake found mean amplification factors at class C sites of about 2 to 3 for the 1- to 10-Hz frequency band (Athanasopoulos and Tikou, 1991; Gazetas *et al.*, 1990; Gariel *et al.*, 1991). Similar amplifications were reported for recordings of the 21 December 1990, Griva earthquake, at station EDE by Pitilakis *et al.* (1992, 1996).

For our applications, we needed frequency-dependent amplifications at all sites. Rather than simply use a constant factor between 2 and 3, as suggested by the studies reviewed above, for class B and C sites, we made use of site amplifications derived by Boore and Joyner (1997) from an extensive strong-motion and borehole dataset, largely in California. For the one class A site (KOZ), underlain by limestone with a thin veneer of colluvium, we judged that the site amplification used by Frankel *et al.* (1996) would be suitable (this amplification is based on a linear velocity gradient near the surface, with $V_{30} = 760$ m/sec, and a deeper velocity profile appropriate for rock sites). The functions $A(f)$ for the three site classes are given in Table 4. The class B amplification is the same as that for an average class B site, as given in Boore and Joyner (1997); the class C amplifications are modifications to Boore and Joyner's average class C amplifications, taking into consideration the observed high-frequency decay of the spectra that we used at class C sites.

It is important to recognize two things about the amplifications in Table 4. First, they represent average amplifications for a number of sites falling within a given site class

Table 4

Site amplifications for stations assigned to indicated site class. Amplifications for other frequencies are obtained by interpolation using linear relations between log amplification and log frequency. These amplifications do not include the effect of attenuation, which must be applied separately. The amplifications may not be appropriate for generic A and C site classes (see text).

Site Class A		Site Class B		Site Class C	
Freq. (Hz)	Ampli.	Freq. (Hz)	Ampli.	Freq. (Hz)	Ampli.
0.01	1.00	0.01	1.00	0.01	1.00
0.10	1.06	0.09	1.21	0.09	1.44
0.24	1.13	0.16	1.32	0.16	1.73
0.45	1.22	0.51	1.59	0.51	2.62
0.79	1.38	0.84	1.77	0.84	3.12
1.38	1.65	1.25	1.96	1.25	3.42
1.93	1.86	2.26	2.25	2.26	3.86
2.85	2.05	3.17	2.42	3.17	4.07
4.03	2.17	6.05	2.70	6.05	5.11
6.34	2.28	16.60	3.25	16.60	5.11
12.54	2.38	61.20	4.15	61.20	5.11
21.23	2.42				
33.39	2.44				
82.00	2.46				

and are not intended to include narrow-band, site-specific resonance effects. Because we used data from particular sites, it would have been preferable to use site-specific amplifications. These were not available for most sites, however. In addition, our goal was to derive parameters that can be used to compute average ground motions for specified magnitudes and distances. As mentioned earlier, we did this by finding $\Delta\sigma$ that best matched the observed spectra over a broad range of frequencies. For this purpose, a generic amplification function is sufficient as long as its average over the frequency range of interest is similar to that of the site-specific amplification. For consistency, ground-motion predictions using the derived $\Delta\sigma$ should also use the same values as we did for the other parameters, including the amplification functions for the various sites.

The second thing to recognize about the amplification functions in Table 4 is that they represent purely elastic amplification, with no loss of energy in the portion of strong shaking due to inelastic energy absorption or scattering of energy into the coda. This is a consequence of our representation of the combined effect of amplification and attenuation as the product of two terms: $A(f)$ in equation (1) and $\exp(-\pi\kappa_0 f)$ in equation (4). This is a matter of computational convenience and seems to capture adequately the combined effect of amplification and attenuation.

Choice of Low-Cut Filters, $I(f)$

The spectra and peak motions were computed from processed data that included low- and high-cut filters. In the modeling, it may be important to include the low-cut filter (the high-cut filter is less important because the frequencies of interest are much less than the high-cut filter frequencies). The cutoff frequencies for the filters as given by the agencies providing the data are included in Table 2 (the filters are linear ramps connecting no-pass and all-pass regions). Note that no information was available for the recording of the 1978 Thessaloniki earthquake, although the records were filtered. According to the information in Table 2, a number of the low-cut filters have rapid cutoffs. While our examination of plots of velocity and displacement waveforms, as well as the Fourier amplitude spectrum, give us confidence that the processed records are not seriously contaminated by noise at the longer periods, we are skeptical that such rapid transitions were actually realized. To determine filter characteristics for the simulations, we fit (by eye) the low-cut filter function used in the simulations to the whole-record Fourier-amplitude spectra. The functional form we used is equivalent to an acausal Butterworth filter:

$$I(f) = 1/(1 + (fcut/f)^{2\times norder}). \quad (5)$$

(An acausal filter is often used in processing strong-motion data to avoid distortions due to phase shifts.) The derived filter parameters *fcut* and *norder* are included in Table 5. The cutoff frequency may be influenced by the earthquake corner frequency. In all cases except for ARG_ARG, *fcut* is at least a factor of 2 lower than the lowest frequency used in determining $\Delta\sigma$, and therefore, any effect of the earthquake corner frequency on *fcut* will not be important for our results. For ARG_ARG, *fcut* is much higher than the expected corner frequency for the earthquake, and *fcut* will not be affected by the earthquake corner frequency.

Results

Measurement of κ and Determination of κ_0

A number of studies have observed that acceleration spectra show a sharp decay at high frequencies (e.g., Hanks, 1982). We modeled this decay with equation (4). In this equation, the κ_0 term is more important than the Q term for small values of the distance r. We estimated κ_0 by using Anderson and Hough's (1984) procedure of fitting a straight line to the natural logarithm of the Fourier-amplitude spectrum as a linear function of frequency. The regression lines were fit between subjectively chosen frequencies of several Hz to near 20 Hz. Each component was considered separately. Figure 3 displays the spectra and the regression fits. In Anderson and Hough's (1984) terminology, the negative value of the slopes of the fitted lines, divided by π, is the parameter κ. The measured values of κ are given in Table 5. These values are in good agreement with others that have been estimated for Greece (Hatzidimitriou *et al.*, 1993; Tselentis, 1993).

The measured value of κ includes site amplification and whole-path attenuation. If we used κ for κ_0 in equation (4), we would be double counting the site amplification and whole-path attenuation, at least as far as the high-frequency

Table 5
Source and Site Parameters Derived from Each Recording

Record Code	Distance (km)* Hyp.	Hor.	Slant	Site Class	k (msrd)**	k_0 (modfd)**	*fcut*†	*norder*†	$\Delta\sigma_1$†† (bars)	$\Delta\sigma_2$†† (bars)	f_0 (Hz)	T_D (sec)	L_f‡ (km)	L_f§ (km)	L_f¶ (km)
THEATHE	30	25	25.4	C	0.056	0.056	0.13	2	54	54	—	—	—	—	—
THEBTHE	30	25	25.4	C	0.056	0.056	0.13	2	50	50	0.17	5.9	29	29	32(1)‖
KOR_KOR	31	13	13.8	C	0.063	0.063	0.08	2	48	48	0.14	7.1	35	41	40(2)‖
ARG_ARG	33	20	20.5	B	0.042	0.047	1.00	15	51	51	0.10	10.	49	52	55(3)‖
KAL_KAL	9	4	6.2	C	0.075	0.076	0.20	2	53	53	0.29	3.5	17	16	15(4)‖
KYL_AML	30	25	25.4	C	0.045	0.046	0.18	2	65	59	0.34	2.9	14	14	17(5)‖
KYL_ZAK	23	15	15.7	C	0.045	0.046	0.16	3	52	59	0.32	3.1	15	14	17(5)‖
GRI_EDE	33	23	23.5	C	0.064	0.064	0.20	2	58	61	0.25	4.0	20	20	15(6)‖
GRI_KIL	43	32	32.3	B	0.063	0.066	0.20	2	64	61	0.26	3.9	19	20	15(6)‖
KOZ_KOZ	27	21	21.5	A	0.034	0.035	0.24	2	63	63	0.16	6.3	31	33	30(7)‖

*"Hyp." is the hypocentral distance; "Hor." is the closest horizontal distance from the station to a point on the Earth's surface that lies directly above the fault rupture; "Slant" is the square root of the sum of the square of "Hor." and the square of the coefficient "h" in Joyner and Boore, 1982 ("h" is period dependent; for illustration, we used 4.7 km, the value for 1-sec period).

**The k(msrd) is the average value of the two horizontal components for each accelerogram; k_0 (modfd) is k(msrd), modified to account for site response and whole-path attenuation.

†The low-cut filter parameters (see text).

††The stress parameter from fitting geometric mean of the horizontal components ($\Delta\sigma_1$) and from averaging $\Delta\sigma_1$ for each earthquake ($\Delta\sigma_2$).

‡Fault-lengths, from duration derived from corner frequency (see text).

§Fault lengths, from equation (11) (Papazachos and Papazachou, 1989).

¶From field observations (including aftershock distributions).

‖Kulhanek and Meyer (1983). (2) Papazachos *et al.* (1984). (3) Scordilis *et al.* (1985). (4) Papazachos *et al.* (1988). (5) Karakostas *et al.* (1993). (6) Panagiotopoulos *et al.* (1993). (7) Papazachos *et al.* (1995).

Table 6
PGV (cm/sec) and PGA (cm/s/s) Records and Simulated

Record Code	Record. PGV	Simulat. PGV	Record. PGA	Simulat. PGA
THEATHE	6.3	6.2	80	74
THEBTHE	14.7	13.8	146	127
KOR_KOR	23.6	26.3	258	269
ARG_ARG	7.5	7.9	151	167
KAL_KAL	28.0	28.0	252	247
KYL_AML	7.5	7.0	119	103
KYL_ZAK	9.8	10.1	146	143
GRI_EDE	10.3	8.4	98	101
GRI_KIL	3.6	3.4	45	46
KOZ_KOZ	7.5	8.4	174	140

diminution of the spectrum is concerned. For this reason, we estimated κ_0 by correcting the measured κ for the effect of the site amplification and whole-path attenuation. We did this by first computing the spectral amplitudes using equation (1) with $\kappa_0 = \kappa$ and the appropriate site amplification from Table 4. We then used the Anderson and Hough (1984) procedure to find κ' for this simulated spectrum, and we obtained κ_0 from the equation

$$\kappa_0 = \kappa + (\kappa - \kappa'). \tag{6}$$

This procedure gives a value for κ_0 that is consistent with the parameters in the simulations and the value of κ obtained from the recordings at each site. We could have estimated κ_0 by dividing the observed spectra by $A(f)D(f)$ before fitting the straight lines. We preferred to keep separate the measured quantity κ and the derived quantity κ_0. The mean values of κ_0 for the two components of each recording (one component for KIL) are given in Table 5; in general, the modifications to κ were very minor.

Based on plots of the relevant variables, we found no systematic dependence of κ_0 on seismic moment and distance.

The combined site amplification and attenuation due to κ_0 are shown in Figure 4, using representative values of κ_0. As we discussed earlier, various studies found site effects (representing the combined effect of amplification and attenuation) between a factor of 1.5 and 3.5 for frequencies between 1 and 10 Hz. Our results are consistent with those studies.

Determination of $\Delta\sigma$

We used the parameters discussed earlier to compute pseudorelative-velocity response spectra (PSV) for a suite of stress parameters. The simulations were done using the random-vibration version of the stochastic model, as given in Boore (1996). The distance we used for each station was given by

$$r = \sqrt{d^2 + h^2}, \tag{7}$$

where d is the closest horizontal distance from the station to a point on the Earth's surface directly above the rupture, and $h(T)$ are the period-dependent pseudodepths determined in the empirical regression analysis of Joyner and Boore

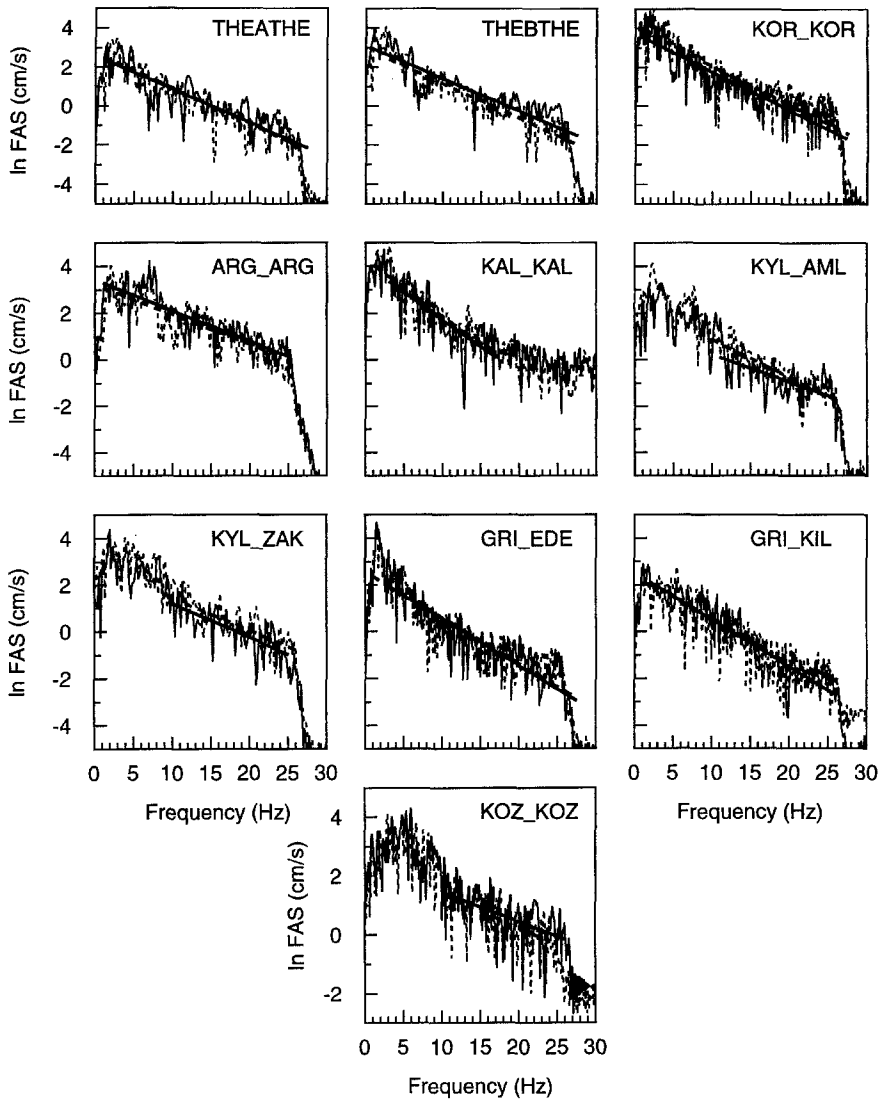

Figure 3. Determination of κ for each horizontal component. The straight lines show the regression fits to ln spectral amplitude versus frequency; the line pattern corresponds to the component (solid for H1, dashed for H2). κ is given by the absolute value of the slope of the line divided by π. The spectra have not been corrected for site amplification or for whole-path attenuation.

(1982). Using these values of $h(T)$ is equivalent to assuming that the depth distribution of the fault rupture and the other factors influencing $h(T)$ is the same for the Greek earthquakes as for those earthquakes used by Joyner and Boore (1982). This seems to be a reasonable assumption; in particular, the depths of the earthquakes (Table 1) are similar to those used by Joyner and Boore (1982). Table 5 gives the hypocentral distance and the distance d. Using d and $h(T)$ instead of epicentral distance and the true focal depth allows a point-source representation of the stochastic model at close distances to an extended rupture (the empirical model, from which $h(T)$ is determined, is also based on a point source). $h(T)$ captures a number of effects, including directivity, possible soil nonlinearity, and fault finiteness. For oscillator periods outside the range of those in the empirical analysis of Joyner and Boore (1982), we assumed that $h(T)$ was constant, with a value given by the end-member values in the empirical analysis.

The simulated and the observed response spectra are plotted in Figure 5 for all recordings considered in this article. Overall, the simulations are in reasonable agreement with the data. An inspection of Figure 5 suggests that a stress parameter of 50 or 60 bars leads to a good fit for all the recordings. We used a simple scheme to find the optimum stress parameter for each recording. The scheme was as follows: we computed the misfit between the average of the logarithms of the two horizontal components and the logarithm of the simulated spectrum for each value of the suite of stress parameters. We then plotted the misfit against stress parameter and chose as the best value of $\Delta\sigma$ the one that

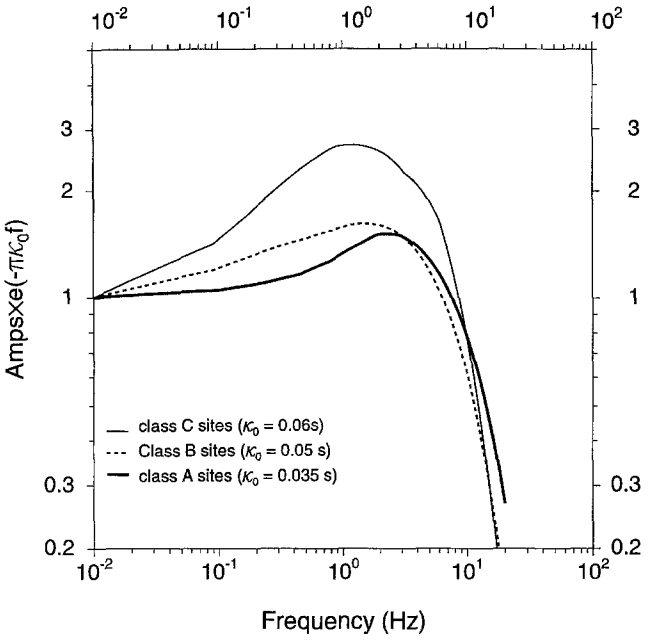

Figure 4. The combined effect of site amplification (Table 4) and attenuation for representative κ_0 for each site class.

minimized the misfit. We used three measures of misfit, in each case summing the following quantity over a subjectively chosen range of oscillator periods: (1) the difference between the logarithms of the observed and simulated response spectrum, (2) the absolute value of the difference between the logarithms of the observed and simulated response spectrum (L1 norm), and (3) the square of the difference between the logarithms of the observed and simulated response spectrum (L2 norm). The periods over which the measure of fit was computed were equally spaced logarithmically, and ranged from 0.1 to 2 sec, with the exception of the recording of the Argostoli earthquake (ARG_ARG), for which the range was 0.1 to 1.0 sec. (Based on prior experience with analog accelerogram records, we have the most confidence in the records for these frequency ranges). Figure 6 shows the various misfit measures as a function of $\Delta\sigma$ for the recordings with the narrowest and broadest minima. Conditional on the various parameters in the model, the stress parameter is surprisingly well determined. The stress parameter from the L2 norm is given in Table 5 for each station ($\Delta\sigma_1$). The average of the stress parameter over all recordings is $\Delta\sigma = 56$, with a formal standard deviation of 6 bars.

Although the stress parameter enters into the simulations through equation (3) for the corner frequency f_0, we emphasize that we are not fitting the corner frequency of the Fourier-amplitude spectrum and then determining $\Delta\sigma$ from f_0. Instead, we are finding the $\Delta\sigma$ that produces the best overall fit to the response spectrum over a range of frequencies, and generally it is the portion of the Fourier spectrum for frequencies greater than the corner frequency that is controlling the level of the response spectra. (This portion of the Fourier spectrum is proportional to $M_0^{1/3}\ \Delta\sigma^{2/3}$.) From $\Delta\sigma$, we can use equation (3) to estimate f_0, and in so doing, there is no inconsistency in our deriving values of f_0 that are lower than the low-cut filters used in the processing (as, for example, for ARG_ARG).

We caution that the optimization process may give a false sense of the accuracy of the derived $\Delta\sigma$, given the uncertainty in the other parameters. For example, an uncertainty in the moment magnitude corresponds to an uncertainty in the derived stress parameter of a factor of 0.9 to 1.1. A more important parameter is the amplification function, which we estimate could be uncertain by 25% to 50% (the distances for some of the recordings could have comparable errors). In the source model used here (equations 2 and 3), the high-frequency spectral level is proportional to $\Delta\sigma^{2/3}$. This means that an uncertainty in $A(f)$ of 25% will lead to an uncertainty in $\Delta\sigma$ of almost 40%; the uncertainty is even larger if the stress parameter is determined for lower-frequency portions of the spectra, which scale with stress less rapidly than $\Delta\sigma^{2/3}$. On the other hand, because all of the parameters are linked together, the uncertainty in predicting ground motion is not as extreme as the uncertainty in the derived parameter $\Delta\sigma$ as long as the predictions are made using the same parameters as were used in deriving $\Delta\sigma$—e.g., if a smaller value of A were used, the best value of $\Delta\sigma$ would increase so that the observed spectra would be predicted equally well. An illustration of this is given in Figure 7, which shows the comparison of simulated and observed response spectra for cases in which there is no site amplification [i.e., $A(f) = 1$] and when the amplification is that discussed earlier. The simulations used the best-fit stresses in each case, which are 53 bars when amplification is included and 415 bars when no amplification is used. The stress parameters differ by a factor of 7.8, although the match to the data is about the same in both cases.

Estimate of Bias in Spectral Model

The model that we used for the simulations clearly is not perfect, as is readily seen in Figures 5 and 7. There could be a number of reasons for this, the most likely of which are that the site amplification in the model is too smooth over the frequency range, not accounting for resonances at individual sites, and that the single-corner-frequency source model is too simple. To quantify the mismatch and search for overall trends, we compute the period-dependent bias between the observed and simulated response spectra. Following Abrahamson *et al.* (1990), the bias factor (BF) is computed as

$$\mathrm{BF}(f) = 10^{\langle \log(\mathrm{obs/sim}) \rangle}, \qquad (8)$$

where $\langle \log(\mathrm{obs/sim}) \rangle$ is the average of the logarithm of the ratio of observed to simulated response spectra at a given period, with the average taken over all recordings. The simulations were made using a stress parameter for each earth-

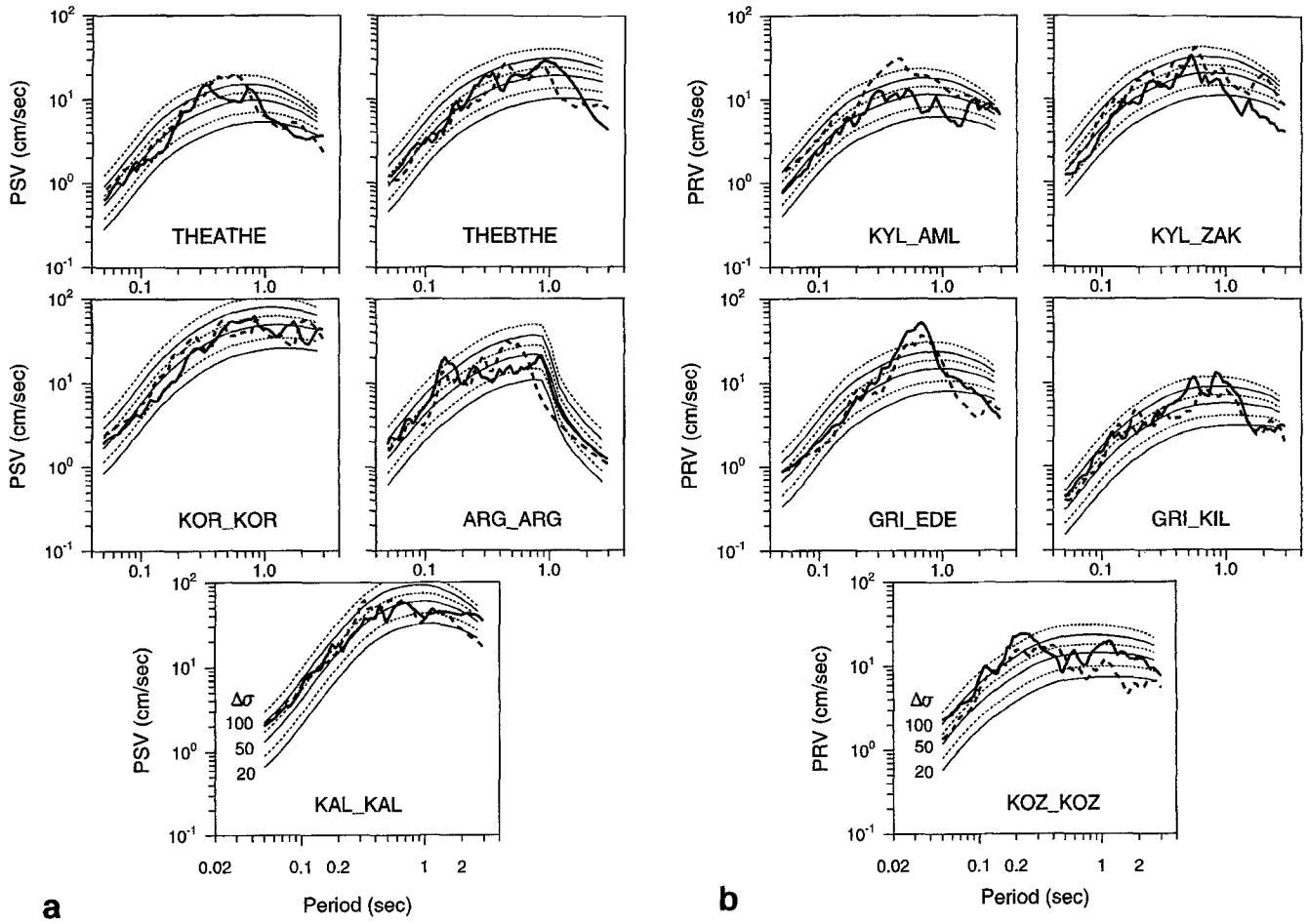

Figure 5. (a, b) Summary plot of PSV spectra from all recordings (10) with simulated curves for a suite of stress parameters (20, 30, 50, 70, 100, and 150 bars). Each plot is labeled with the earthquake code and the station code, as given in Tables 1 and 2 (e.g., "KYL_AML" is the Kyllini earthquake recorded at Amaliada). The thick lines are the response spectra computed from the observed horizontal components (solid: component H1; dashed: component H2). The simulated spectra include the low-frequency cutoffs used in processing the recorded data. Although high-cut filters were employed in the data processing, they have not been included in the simulations.

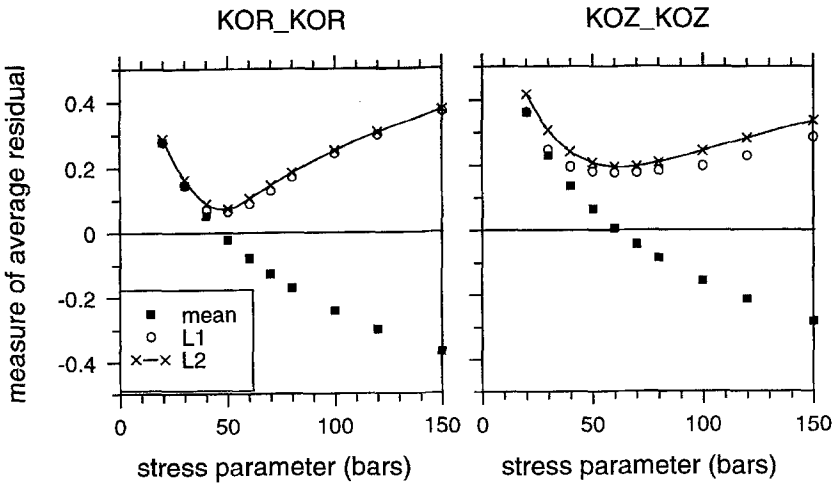

Figure 6. Examples of determining $\Delta\sigma$ by using various measures of misfit between observed and simulated response spectra. Shown are the best (KOR_KOR) and worst (KOZ_KOZ) constrained values of $\Delta\sigma$. The various measures were calculated between periods of 0.1 and 2 sec.

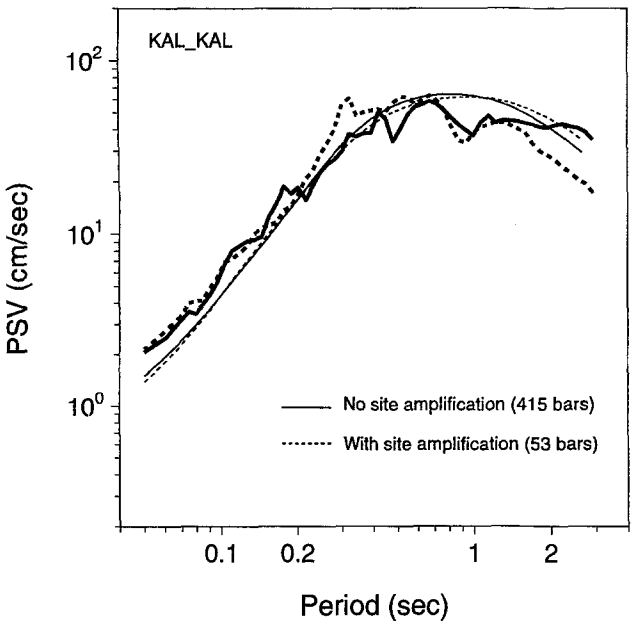

Figure 7. Example of importance of the site amplification on the derived stress parameter, for the KAL_KAL recording. The light solid and dashed lines are simulated response spectra with and without amplification, respectively. The thick lines are the response spectra computed from the observed horizontal components (solid: component H1; dashed: component H2). The best-fit stress parameter is 53 bars with amplification and 415 bars without amplification.

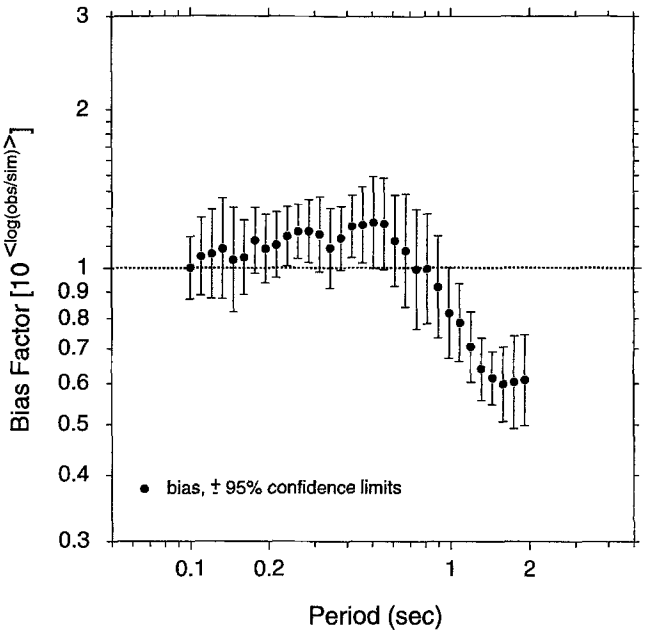

Figure 8. The bias factor obtained from the average over all recordings of the logarithm of the ratio between the observed and simulated response spectra.

quake given by the average of the best-fit stress parameters from each recording ($\Delta\sigma_2$ in Table 5). The bias factor, shown with its 95% confidence limits in Figure 8, has some clear trends (an unbiased prediction would have a bias factor of unity). The most obvious feature is the overprediction of the observations at long periods (a bias less than 1.0). We doubt that this is a result of long-period noise in the observations, which if present would tend to increase the bias factor (and, in addition, we judge the data to have little noise for the periods used). A bias factor less than 1.0 is commonly seen in point-source stochastic simulations of data (e.g., EPRI, 1993; W. Silva, written comm., 1996) and may be due to the point-source assumption or may be a reflection of the simple source spectrum in the model. We doubt that this is due to noise, which would have increased the observations. We find a small and relatively constant bias for periods less than about 0.8 sec, such that the simulations underpredict the observations by about a factor of 0.9. Because we used periods from 0.1 to 2.0 sec in determining $\Delta\sigma$, the bias must be positive for short periods in order to compensate for the large negative bias at longer periods. The short-period bias, already small, would be smaller still if we had restricted the periods used in determining $\Delta\sigma$ to be less than 1.0 sec.

Consistency of $\Delta\sigma$ with PGV, PGA, Rupture Duration, and Fault Length

The stress parameter $\Delta\sigma$ was obtained by fitting observed response spectra. In this section, we compare other measures of ground motion and fault parameters to predictions made with the derived $\Delta\sigma$.

The first comparisons are with the two other measures of ground motion: peak velocity (PGV) and peak acceleration (PGA). These measures of ground motion were computed using the same stochastic model and parameters used to compute the response spectra; a comparison of simulated and measured values is given in Figure 9. On the basis of this comparison, we judge the derived $\Delta\sigma$ to be consistent with the PGV and PGA.

The second comparisons are with measures of rupture duration, T_d, and fault length, L_f. In this study, we use equation (3) in order to compute the corner frequencies, f_0, for each earthquake. This calculation is carried out for the best-fit stress parameters for each earthquake. We used Hanks and McGuire's (1981) relation $T_d = 1/f_0$ to compute the rupture durations T_d. The calculated corner frequencies f_0 and rupture durations T_d are given in Table 5. For the double event of the 20 June 1978, Thessaloniki earthquake, we calculated the source parameters only for event B, in order to compare to other available methods for the strong earthquake. The f_0 values are in good agreement with those that have been calculated for the same earthquakes in Greece using different methods (Papastamatiou *et al.*, 1993). Using observations and assuming a logarithmic dependence of rup-

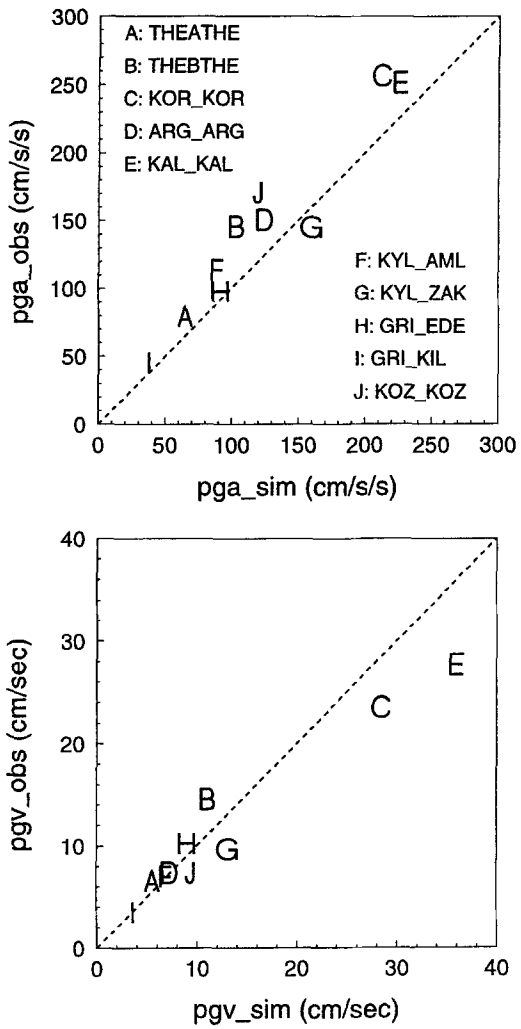

Figure 9. Scatter plot of observed and simulated peak acceleration and peak velocity. Symbols correspond to the earthquake and station pairs indicated by the codes (see Tables 1 and 2). The simulations use the best-fit stress parameters for each earthquake, as given by $\Delta\sigma_2$ in Table 5.

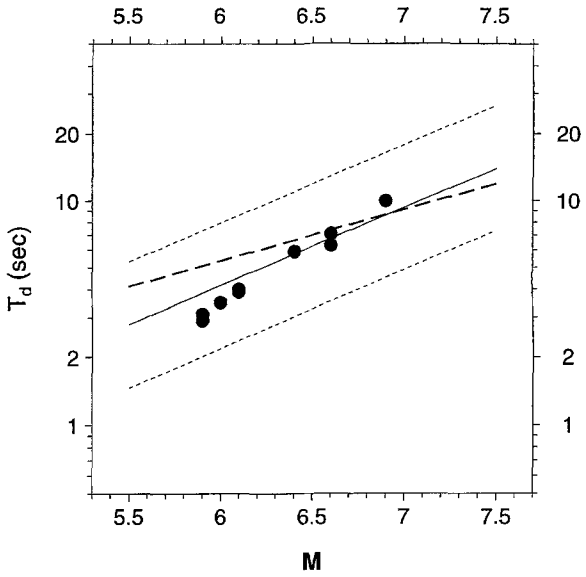

Figure 10. Durations versus moment magnitude. The filled circles are simulations using the best-fit stress parameters (Table 5) for each earthquake, the thin lines are mean $\pm 1\sigma$ bracketed durations proposed by Papazachos *et al.* (1992), and the thick dashed line is the rupture time proposed by Papazachos and Papazachou (1989).

ture time T, on magnitude **M**, the following relation has been proposed by Papazachos and Papazachou (1989):

$$\log T = -0.65 + 0.23\mathbf{M}. \quad (9)$$

Papazachos *et al.* (1992), using the main body of the Greek strong-motion data, estimated the bracketed duration B_D for the same region. The logarithmic dependence of the bracketed duration B_D on magnitude **M** was studied, and the following relation was proposed:

$$\log B_D = -1.48 + 0.35\mathbf{M} \pm 0.28. \quad (10)$$

Both the rupture time T and bracketed duration B_D ($\pm 1\sigma$), are shown in Figure 10. The rupture durations T_d derived from the stress parameters of the seven earthquakes are also shown in Figure 10. There is good agreement between the various durations.

Using the values of the rupture duration T_d, which were calculated for the stress parameter for each earthquake, the fault lengths L_f were computed from the equation $L_f = 2.0v_rT_d$. The rupture velocity, v_r, was given a value of $0.72\beta = 2.45$ km/sec (Papazachos, 1990). The factor of 2 in the equation is due to the bilateral rupture of all the earthquakes studied in this article, as revealed by the locations of aftershocks. The results are given in the third to last column in Table 5. For comparison, the second to last column contains fault lengths obtained from the empirical relation

$$\log L_f = -1.85 + 0.51\mathbf{M}, \quad (11)$$

proposed by Papazachos and Papazachou (1989) for earthquakes in Greece, and the last column contains fault lengths measured in the field. The table shows good agreement between the various estimates of fault length.

Discussion and Conclusions

We fit a single-corner-frequency ω^{-2} source model to response spectra from recordings of eight of the largest recent earthquakes in Greece. We found a mean stress parameter ($\Delta\sigma$) of 56 bars, with little variation from one earthquake to another (the range was 48 to 63 bars). As part of the analysis, the diminution parameter κ_0 was determined for each recording site. For a typical site, the value was about

0.06. The value of $\Delta\sigma$ is conditional on the site amplification used in the simulations. Based on several studies at strong-motion stations in Greece, as well as strong-motion and borehole shear-wave velocity in California, we used a site amplification function that gave a total site effect (when combined with attenuation) of about a factor of 2.5 for the most numerous soil sites. The total site effect for the stiffer sites had a maximum amplitude of about a factor of 1.5.

We found a distinct bias in our results, such that on the average, the simple stochastic, point-source model with an average, smoothed site amplification and single corner-frequency source spectra underpredicts the response spectra for periods between 0.1 and 0.8 sec by a factor of about 0.9 and overpredicts the spectra for periods longer than 0.8 sec (by a factor of about 1.7 at a period of 2.0 sec). This bias can be taken as a correction factor in predicting motions for future earthquakes.

Predictions of peak velocity, peak acceleration, rupture duration, and fault length made using the parameters derived from fitting the response spectra are in good agreement with observations.

The relatively constant value of $\Delta\sigma$ and the consistency of the predictions with several measures of ground motion and fault characteristics encourages us that the results in this article can form the basis for predicting ground motions at sites in Greece for which there are no strong-motion recordings. For consistency, any such predictions must use all of the parameters in our model, including site amplification and κ_0, rather than just $\Delta\sigma$. Recent empirical regression analyses of strong-motion data from around the world finds that ground motion is a function of the type of faulting, with reverse-slip faulting generally producing larger motions than strike-slip or normal faulting (Abrahamson and Shedlock, 1997, and articles referenced therein). This might imply that the stress parameter is a function of the type of faulting. Almost all of the earthquakes considered in this article had normal faulting mechanisms, so we could not investigate a mechanism dependence for the stress parameter. In view of the possibility of a mechanism dependence, however, we caution the reader that the stress parameter determined in this article may not be applicable for reverse-slip earthquakes.

Acknowledgments

The main part of this work was carried out when one of the authors (B.N.M.) was a visitor at USGS, Menlo Park, California. That author expresses his sincere gratitude to U.S. Geological Survey for the accommodation and general help during this work. Special thanks are due to Drs. W. Joyner, P. Spudich, and J. Boatwright for their useful comments and discussions. Eleni Louvari from Geophysical Lab of Aristotle University of Thessaloniki and C. Papazachos kindly provided Figure 1. We thank W. Joyner, S. Hartzell, B. C. Papazachos, and two anonymous reviewers for thoughtful reviews of the manuscript. This work was supported by the U.S. Nuclear Regulatory Commission and the EEC Environmental EV5V-CT94-0513 research project and ITSAK IS/1130/10-14-1994 research project.

References

Abrahamson, N. A. and K. M. Shedlock (1997). Overview, *Seism. Res. Lett.* **68,** 9–23.

Abrahamson, N. A., P. G. Somerville, and C. A. Cornell (1990). Uncertainty in numerical strong motion predictions, *Proc. of the 4th U.S. National Conference on Earthquake Engineering,* Palm Springs, California, Vol. 1, 407–416.

Anagnostopoulos, S. A., B. N. Margaris, N. P. Theodulidis, E. E. Vorrias, and A. I. Marinos (1985). Strong motion bulletin of ITSAK network (Time Period 1980–1985), Inst. Eng. Seism. Earthquake Eng., Rept. ITSAK:85-01, 1–42.

Anagnostopoulos, S. A., D. Rinaldis, V. A. Lekidis, B. N. Margaris, and N. P. Theodulidis (1987). The Kalamata, Greece, earthquake of September 13, 1986, *Earthquake Spectra* **3,** 365–402.

Anderson, J. G. and S. E. Hough (1984). A model for the shape of the Fourier spectrum of acceleration at high frequencies, *Bull. Seism. Soc. Am.* **74,** 1969–1993.

Athanasopoulos, G. A. and M. Tikou (1991). Site dependent ground response for the 1986 Kalamata earthquakes, in *Proc. Inter. Conf. Earthquake Resistant Construction and Design,* Berlin, 21–32.

Atkinson, G. M. and D. M. Boore (1997). Some comparisons between recent ground-motion relations, *Seism. Res. Lett.* **68,** 24–40.

Atkinson, G. M. and W. Silva (1997). An empirical study of earthquake source spectra for California earthquakes, *Bull. Seism. Soc. Am.* **87,** 97–113.

Boore, D. M. (1983). Stochastic simulation of high-frequency ground motion based on seismological models of the radiated spectra, *Bull. Seism. Soc. Am.* **73,** 1865–1894.

Boore, D. M. (1984). Use of seismoscope records to determine ML and peak velocities, *Bull. Seism. Soc. Am.* **74,** 315–324.

Boore, D. M. (1996). SMSIM—Fortran programs for simulating ground motions from earthquakes: version 1.0, *U.S. Geol. Surv. Open-File Rept. 96-80-A* and *96-80-B,* 73 pp.

Boore, D. M. and G. A. Atkinson (1987). Stochastic prediction of ground motion and spectral response parameters at hard-rock sites in Eastern North America, *Bull. Seism. Soc. Am.* **77,** 440–467.

Boore, D. M. and G. M. Atkinson (1989). Spectral scaling of the 1985 to 1988 Nahanni, Northwest Territories, earthquakes, *Bull. Seism. Soc. Am.* **79,** 1736–1761.

Boore, D. M. and W. B. Joyner (1997). Site amplifications for generic rock sites, *Bull. Seism. Soc. Am.* **87,** 327–341.

Boore, D. M., W. B. Joyner, and T. E. Fumal (1993). Estimation of response spectra and peak accelerations from Western North American Earthquakes: An interim report, *U.S. Geol. Surv. Open-File Rept. 93-509,* 1–72.

Carydis, P. G., N. R. Tilford, G. E. Brandow, and J. O. Jirsa (1982). The central Greece earthquakes of February–March 1981. *A Reconnaissance and Engineering Report,* Academic Press, Washington, D.C., 1–160.

Carydis, P., J. Drakopoulos, S. Pantazopoulou, and J. Taflambas (1983). Evaluation of the June 20 and July 5, 1978, Thessaloniki strong motion records, in The Thessaloniki Northern Greece, earthquake of June 20, 1978 and its sequence, Technical Chamber of Greece, 231–256.

Electric Power Research Institute (EPRI) (1993). Guidelines for determining design basis ground motions, Electric Power Research Institute, Palo Alto, California, Rept. No. EPRI TR-102293 (5 volumes).

Frankel, A., C. Mueller, T. Barnhard, D. Perkins, E. V. Leyendecker, N. Dickman, S. Hanson, and M. Hopper (1996). National seismic hazard maps, June 1996 documentation, *U.S. Geol. Surv. Open-File Rept. 96-532.*

Gariel, J.-C., P.-Y. Bard, and K. Pitilakis (1991). A theoretical investigation of source, path and site effects during the 1986 Kalamata earthquake (Greece), *Geophys. J. Int.* **104,** 165–177.

Gazetas, G., P. Dakoulas, and A. Papageorgiou (1990). Local-soil and source-mechanism effects in the 1986 Kalamata (Greece) earthquake, *Earthquake Eng. Struct. Dyn.* **19,** 431–456.

Hanks, T. C. (1982). fmax, *Bull. Seism. Soc. Am.* **72,** 1867–1879.

Hanks, T. C. and R. K. McGuire (1981). The character of high-frequency strong ground motion, *Bull. Seism. Soc. Am.* **71,** 2071–2095.

Hatzidimitriou, P. M. (1993). Attenuation of coda waves in northern Greece, *Pageoph* **140,** 63–78.

Hatzidimitriou, P. M. (1995). S-wave attenuation in the crust in northern Greece, *Bull. Seism. Soc. Am.* **85,** 1381–1387.

Hatzidimitriou, P., C. Papazachos, A. Kiratzi, and N. Theodulidis (1993). Estimation of attenuation structure and local earthquake magnitude based on acceleration records in Greece, *Tectonophysics* **217,** 243–253.

Joyner, W. B. (1984). A scaling law for the spectra of large earthquakes, *Bull. Seism. Soc. Am.* **74,** 1167–1188.

Joyner, W. B. and D. M. Boore (1982). Prediction of earthquake response spectra, *Proc. 51st Ann. Convention Structural Eng. Assoc. of Cal.,* also *U.S. Geol. Surv. Open-File Rept. 82-977,* 16 pp.

Joyner, W. B. and D. M. Boore (1988). Measurement, characterization, and prediction of strong ground motion, in *Proc. Earthquake Eng. Soil Dyn. II, GT Div/ASCE,* Park City, Utah, 1988, 43–102.

Karakostas, B. G., E. M. Scordilis, Ch. A. Papaioannou, B. C. Papazachos, and D. Mountrakis (1993). Focal properties of the October 16, 1988 Killini earthquake (western Greece), in *Proc. 2nd Congr. of the Hellenic Geophys. Union,* Florina, 1993, Vol. 1, 136–145.

Kulhanek, O. and K. Meyer (1983). Spectral study of the June 20, 1978, Thessaloniki earthquake, in The Thessaloniki Northern Greece, earthquake of June 20, 1978 and its sequence, Technical Chamber of Greece, 187–200.

Lachet, C., P.-Y. Bard, D. Hatzfeld, C. Papaioannou, M. Scordilis, T. Hatzidimitriou, N. Theodulidis, and B. Margaris (1995). An experimental study of the microzonation in the city of Thessaloniki (Greece), in *Proc. of the 5th International Conference on Seism. Zonation,* Nice, 1995, Vol. II, 1619–1626.

Margaris, B. N., A. Marinos, N. Theodulidis, E. Vorrias, and A. Akritidis (1990). ITSAK strong motion bulletin (1986–1988), Inst. Eng. Seism. Earthquake Eng., Rept ITSAK:90-01, 1–89.

Margaris, B., N. Theodulidis, I. Kalogeras, and D. Papastamatiou (1993). Strong motion records of the Kyllini seismic sequence (October 16, 1988), Inst. Eng. Seism. Earthquake Eng., Rept ITSAK: 93-16, 1–13.

Panagiotopoulos, D. G., E. E. Papadimitriou, Ch. A. Papaioannou, E. M. Scordilis, and B. C. Papazachos (1993). Source properties of the 21 December 1990 Goumenissa earthquake in northern Greece, in *Proc. of the 2nd Congr. of the Hellenic Geophys. Union,* Florina, 1993, Vol. 1, 286–296.

Papastamatiou, D., B. Margaris, and N. Theodulidis (1993). Estimation of the parameters controlling strong ground motion from shallow earthquakes in Greece, in *Proc. of the 2nd Congr. of the Hellenic Geophys. Union,* Florina, 1993, Vol. 1, 192–201.

Papazachos, B. (1990). *Introduction to Seismology,* Ziti Publishing Co., 382 pp. (in Greek).

Papazachos, B. and C. Papazachou (1989). The Earthquakes in Greece, Ziti Publishing Co., 356 pp. (in Greek).

Papazachos, B., D. Mountrakis, A. Psilovikos, and G. N. Leventakis (1980). Focal properties of the 1978 earthquakes in the Thessaloniki area, *Bulgarian Geophys. J.* **6,** 72–80.

Papazachos, B. C., P. E. Comninakis, E. E. Papadimitriou, and E. M. Scordilis (1984). Properties of the February–March 1981 seismic sequence in the Alkyonides gulf of central Greece, *Ann. Geophys.* **2,** 537–544.

Papazachos, B., A. Kiratzi, B. Karakostas, D. Panagiotopoulos, E. Scordilis, and D. M. Mountrakis (1988). Surface fault traces, fault plane solution and spatial distribution of the aftershock of the September 13, 1986 earthquake of Kalamata (Southern Greece), *Pageoph* **126,** 55–68.

Papazachos, B. C., B. N. Margaris, N. P. Theodulidis, and Ch. A. Papaioannou (1992). Seismic hazard assessment in Greece based on strong motion duration, in *Proc. of the 10th WCEE,* Madrid, Vol. 1, 425–430.

Papazachos, B. C., D. G. Panagiotopoulos, E. M. Scordilis, F. Karakaisis, Ch. A. Papaioannou, B. G. Karakostas, E. E. Papadimitriou, A. A. Kiratzi, P. M. Hatzidimitriou, G. N. Leventakis, Ph. S. Voidomatis, K. I. Peftitselis, and T. M. Tsapanos (1995). Focal properties of the 13 May 1995 large (Ms = 6.6) earthquake in the Kozani area (North Greece), *Aristotle Univ. Thessaloniki Publ.* **4,** 1–13.

Papazachos, B. C., A. A. Kiratzi, and B. G. Karakostas (1997). Toward a homogeneous moment magnitude determination for earthquakes in Greece and surrounding area, *Bull. Seism. Soc. Am.* **87,** 474–483.

Pitilakis, K., B. Margaris, V. Lekidis, N. Theodulidis, and A. Anastasiadis (1992). The Griva, northern Greece, earthquake of December 21, 1990. (Seismological, structural and geotechnical aspects), *European Earthquake Eng.* **2.92,** 20–35.

Pitilakis, K., T. Hatzigogos, T. Tika, C. Lotgetidis, D. Raptakis, S. Tolis, E. Tsaroucha, E. Karaolani, I. Livadiotis, N. Theodulidis, B. Margaris, V. Lekidis, A. Akritidis, E. Vorias, A. Marinos, N. Kaltetziotis, N. Sabatakakis, and G. Tsiabaos (1996). Study of the effects of local soil conditions; geomorphology and dynamic soil-structure interaction of the instrumental recordings of the National strong motion network, Earthquake Protection Planning Organization, Final Project Report (in Greek).

Raptakis, D., E. Karaolani, K. Pitilakis, and N. Theodulidis (1994). Horizontal to vertical spectral ratio and geological conditions: The case of downhole array in Thessaloniki (Greece), in *Proc. XXIV Gen. Assembly of Eur. Seism. Comm.,* Athens, 1994, Vol. III, 1570–1578.

Scordilis, E. M., G. F. Karakaisis, B. G. Karakostas, D. G. Panagiotopoulos, P. E. Comninakis, and B. C. Papazachos (1985). Evidence for transform faulting in the Ionian Sea: the Cephalonian island earthquake sequence of 1983, *Pageoph* **123,** 387–397.

Soufleris, C. and G. Stewart (1981). A source study of the Thessaloniki (northern Greece) 1978 earthquake sequence, *Geophys. J. R. Astr. Soc.* **67,** 343–358.

Stavrakakis, G., I. S. Kalogeras, and J. C. Drakopoulos (1992). Preliminary analysis of Greek accelerograms recorded at stations of NOA's network. Time Period 1973–1990, National Observ. Athens, *Geodynamic Inst.* **4,** 1–37.

Theodulidis, N. and V. Lekidis (1996). The Kozani-Grevena, Northern Greece, earthquake of May 13, 1995: strong motion data and structural response, *J. of European Earthquake Eng.* **1,** 3–13.

Theodulidis, N. P. and B. C. Papazachos (1992). Dependence of strong ground motion on magnitude-distance, site geology and macroseismic intensity for shallow earthquakes in Greece: I, Peak horizontal acceleration, velocity and displacement, *Soil Dyn. Earthquake Eng.* **11,** 387–402.

Theodulidis, N. P., B. N. Margaris, and D. I. Papastamatiou (1986). Planning of accelerographic network, Inst. Eng. Seism. Earthquake Eng., Rept. ITSAK: 86-04, 1–148.

Toro, G. R., N. A. Abrahamson, and J. F. Schneider (1997). Model of strong ground motions from earthquakes in central and eastern North America: best estimates and uncertainties, *Seism. Res. Lett.* **68,** 41–57.

Trifunac, M. D. and G. Brady (1975). On the correlation of seismic intensity scales with peaks of recorded strong ground motion, *Bull. Seism. Soc. Am.* **65,** 139–162.

Tselentis, G.-A. (1993). Shallow attenuation in the west Corinth-Patras rift, Greece, *Bull. Seism. Soc. Am.* **83,** 603–609.

Institute of Engineering Seismology and Earthquake Engineering (ITSAK)
P.O. Box 53, GR 55 102, Finikas
Thessaloniki, Greece
E-mail: margaris@itsak.gr
(B.N.M)

U.S. Geological Survey
Menlo Park, California 94025
E-mail: boore@samoa.wr.usgs.gov
(D.M.B)

Manuscript received 24 February 1997.